The effect of pulse width on the dynamics of pulse-coupled oscillators

Afifurrahman,[1, a)] Ekkehard Ullner,[1, b)] and Antonio Politi[1, c)]
Institute for Pure and Applied Mathematics and Department of Physics (SUPA), Old Aberdeen, Aberdeen, AB24 3UE, United Kingdom

(Dated: 30 January 2021)

The idealisation of neuronal pulses as δ-spikes is a convenient approach in neuroscience but can sometimes lead to erroneous conclusions. We investigate the effect of a finite pulse-width on the dynamics of balanced neuronal networks. In particular, we study two populations of identical excitatory and inhibitory neurons in a random network of phase oscillators coupled through exponential pulses with different widths. We consider three coupling functions, inspired by leaky integrate-and-fire neurons with delay and type-I phase-response curves. By exploring the role of the pulse-widths for different coupling strengths we find a robust collective irregular dynamics, which collapses onto a fully synchronous regime if the inhibitory pulses are sufficiently wider than the excitatory ones. The transition to synchrony is accompanied by hysteretic phenomena (i.e. the co-existence of collective irregular and synchronous dynamics). Our numerical results are supported by a detailed scaling and stability analysis of the fully synchronous solution. A conjectured first-order phase transition emerging for δ-spikes is smoothed out for finite-width pulses.

Neuronal networks with a nearly balanced excitatory/inhibitory activity evoke significant interest in neuroscience due to the resulting emergence of strong fluctuations akin to those observed in the resting state of the mammalian brain. While most studies are limited to a δ-like pulse setup, much less is known about the collective behavior in the presence of finite pulse-widths. In this paper, we investigate exponential pulses, with the goal of testing the robustness of previously identified regimes such as the spontaneous emergence of collective irregular dynamics (CID). Moreover, the finite-width assumption paves the way to the investigation of a new ingredient, present in real neuronal networks: the asymmetry between excitatory and inhibitory pulses. Our numerical studies confirm the emergence of CID also in the presence of finite pulse-width, although with a couple of warnings: (i) the amplitude of the collective fluctuations decreases significantly when the pulse-width is comparable to the interspike interval; (ii) CID collapses onto a fully synchronous regime when the inhibitory pulses are sufficient longer than the excitatory ones. Both restrictions are compatible with the recorded behavior of real neurons. Additionally, we find that a seemingly first-order phase transition to a (quasi)-synchronous regime disappears in the presence of a finite width, confirming the peculiarity of the δ-spikes. A transition to synchrony is instead observed upon increasing the ratio between the width of inhibitory and excitatory pulses: this transition is accompanied by a hysteretic region, which shrinks upon increasing the network size. Interestingly, for a connectivity comparable to that of the mammalian brain, such a finite-size effect is still sizable. Our numerical studies might help to understand abnormal synchronisation in neurological disorders.

[a)]Electronic mail: r01a17@abdn.ac.uk
[b)]Electronic mail: e.ullner@abdn.ac.uk
[c)]Electronic mail: a.politi@abdn.ac.uk

I. INTRODUCTION

Irregular firing activity is a robust phenomenon observed in certain areas of mammalian brain such as hippocampus or cortical neurons[1,2]. It plays a key role for the brain functioning in the visual and prefrontal cortex. This behavior does not only emerge from intrinsic properties of the single neuronal cells, but it can also arise from the combined action of many interacting units[3,4].

Several numerical and theoretical studies of minimal models have been performed to uncover the underlying mechanisms. In binary networks, for instance, the irregular activity was hypothesized to be the result of a (statistical) balance between excitation and inhibition[5]. The resulting balanced state[6] is characterized by a constant (on average) firing rate accompanied by irregular fluctuations, which can treated as stochastic-like. In fact, this idea allowed Brunel[7] to develop a powerful analytical method to describe a more realistic model of leaky integrate-and-fire (LIF) neurons. Altogether this regime can be seen as a fluctuating asynchronous state, with negligible correlations among the various neurons.

A numerical study of an ensemble of heterogeneous LIF neurons with delay has independently revealed that irregular activity can also emerge in a strictly-inhibitory environment[8]. This self-sustained regime, that we call "collective irregular dynamics" (CID), differs from the asynchronous regime in that the temporal fluctuations persist in the so-called thermodynamic limit, when the number N of neurons is let diverge to infinity[9,10]. In other words, we are in the presence of a collective phenomenon, akin to partially synchronized states[11]. The robustness of the mechanism has been confirmed by further studies of pulse-coupled phase oscillators[12] in the absence of delay.

The stochastic-like dynamics in CID can be of different types: (i) the manifestation of low-dimensional chaos in the presence of two distinct populations[13]; (ii) high-dimensional chaos for a single population of oscillators[12]; (iii) stable chaos found in a diluted network of LIF[14] and in more disordered setups[15,16]. Stable chaos is a form of irregular dynamics, which emerges in the presence of negative Lyapunov expo-

nents[17] akin to the behavior of chaotic cellular automata.

Recently, it has been shown that CID arises also in the typical balanced setup, under the condition of small unbalance and in the limit of massive coupling (finite connectivity density)[9,10]. It is therefore of utmost importance to test the robustness of such a phenomenon, by exploring more realistic setups. In this paper we explore the role played by the spike-width. Most of the numerical studies found in the literature deal with δ-spikes. This is an idealization, typically prompted by the easiness of the related simulations, but it has its own limits. First, real pulses have a small but finite width[18]. Second, it has been shown that the stability of some synchronous regimes of LIF neurons may qualitatively change when arbitrarily short pulses are considered (in the thermodynamic limit)[19]. For this reason, it is wise to extend the analysis of CID to networks of neurons interacting via finite-width pulses.

A preliminary study has been already published in Ref. [20], where the authors have not performed any finite-size scaling analysis and, more important, no any test of the presence of CID has been carried out. Here we study a system composed of two populations of (identical) excitatory and inhibitory neurons, which interact via exponential pulses of different width, as it happens in real neurons[21].

Handling pulses with a finite width requires two additional variables per single neuron, in order to describe the evolution of the incoming excitatory and inhibitory fields. The corresponding mathematical setup has been recently studied in Ref. [22] with the goal of determining the stability of the fully synchronous state in a sparse network. The presence of two different pulse-widths leads to non-intuitive stability properties, because the different time dependence of the two pulses may change the excitatory/inhibitory character of the overall field perceived by each single neuron. Here, we basically follow the same setup introduced in Ref. [22] with the main difference of a massively coupled network, to be able to perform a comparative analysis of CID.

The randomness of the network accompanied by the presence of three variables per neuron, makes an analytical treatment quite challenging. For this reason we limit ourselves to a numerical analysis. However, we accompany our studies with a careful finite-size scaling to extrapolate the behavior of more realistic (larger) networks. Our first result is that CID is observed also in the presence of finite pulse-width, although we also find a transition to full synchrony when the inhibitory pulses are sufficiently longer than excitatory ones. The transition is first-order (discontinuous) and is accompanied by hysteresis: there exists a finite range of pulse-widths where CID and synchrony coexist.

The finite-size analysis suggests that in the thermodynamic limit CID is not stable when the pulse-width of inhibitory neurons is strictly longer than that of the excitatory ones. However, the convergence is rather slow and we cannot exclude that the asymmetry plays an important role in real neuronal networks of finite size.

The remainder of this paper is organized as follows. In section II, we define the model, including the phase response curves (PRCs) used in our numerical simulation. In the same section we also introduce the tools and indicators later used to characterize the dynamical regimes, notably an order parameter to quantify the degree of synchronization[23]. In section III, we present some results obtained for strictly δ pulses to test robustness of CID in our context of coupled phase oscillators. In Sec. IV we discuss the symmetric cases of identical finite pulse-widths. Sec. V is devoted to a thorough analysis of CID by varying the finite pulse-widths. Sec. VI contains a discussion of the transition region, intermediate between standard CID and full synchrony. In the same section, the robustness of the transition region is analysed, by considering different PRCs. Finally, section VII is devoted to the conclusions and a brief survey of the open problems.

II. MODEL

Our object of study is a network of N phase oscillators (also referred to as neurons), the first $N_e = bN$ being excitatory, the last $N_i = (1-b)N$ inhibitory (obviously, $N_e + N_i = N$). Each neuron is characterized by the phase-like variable $\Phi^j \leq 1$ (formally equivalent to a membrane potential), while the (directed) synaptic connections are represented by the connectivity matrix $\mathbf{G}$ with entries

$$G_{j,k} = \begin{cases} 1, & \text{if } k \to j \text{ active} \\ 0, & \text{otherwise} \end{cases}$$

where $\sum_{k=1}^{N_e} G_{j,k} = K_e$ and $\sum_{k=N_e+1}^{N} G_{j,k} = K_i$, meaning that each neuron j is characterized by the same number of incoming excitatory and inhibitory connections, as customary assumed in the literature[24] ($K = K_e + K_i$ represents the connectivity altogether). Here, we assume that K is proportional to N, that is $K = cN$, i.e. we refer to massive connectivity. Further, the network structure is without autapse, i.e. $G_{j,j} = 0$.

The evolution of the phase of both excitatory and inhibitory neurons is ruled by the same equation,

$$\dot{\Phi}^j = 1 + \frac{\mu}{\sqrt{K}} \Gamma\left(\Phi^j\right)\left(E^j - I^j\right), \tag{1}$$

where $E^j(I^j)$ the excitatory (inhibitory) field perceived by the jth neuron, while $\Gamma(\Phi)$ represents the phase-response curve (PRC) assumed equal for all neurons; finally, μ is the coupling strength. Whenever Φ^k reaches the threshold $\Phi_{th} = 1$, it is reset to the value $\Phi_r = 0$ and enters a refractory period t_r during which it stands still and is insensitive to the action of both fields. The fields E^j and I^j are the linear superposition of exponential spikes emitted by the upstream neurons. Mathematically,

$$\begin{aligned} \dot{E}^j &= -\alpha\left(E^j - \sum_n G_{j,k} P_k \delta(t - t_n^k)\right) \\ \dot{I}^j &= -\beta\left(I^j - g\sum_n G_{j,k}(1-P_k)\delta(t - t_n^k)\right), \end{aligned} \tag{2}$$

where α (β) denotes the inverse pulse-width of the excitatory (inhibitory) spikes and t_n^k is the emission time of the nth spike emitted by the kth neuron. The coefficient g accounts for the

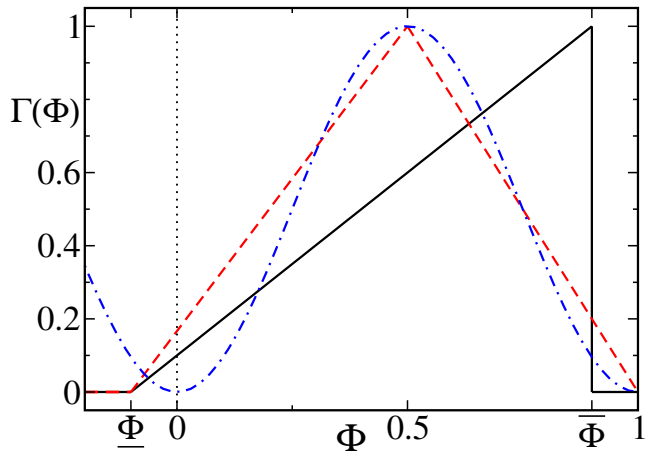

FIG. 1. Example of the phase response curves (PRCs): PRC_1 with $\underline{\Phi} = -0.1$ and $\overline{\Phi} = 0.9$ (black line), PRC_2 (red dashed line), PRC_3 (blue dashed and dot line). The vertical dot line refers to the reset membrane potential ($\Phi_r = 0$).

relative strength of inhibition compared to excitation. $P_k = 1$ if the kth neuron is excitatory, otherwise $P_k = 0$.

In the limit of $\alpha(\beta) \to \infty$ (δ-spikes) both fields can be expressed as simple sums

$$E^j = \sum_n G_{j,k} P_{,k} \delta(t - t_n^k) \tag{3}$$
$$I^j = g \sum_n G_{j,k} (1 - P_k) \delta(t - t_n^k) .$$

Let us now introduce the PRCs used later in our numerical simulations. We consider three different shapes:

- PRC_1

$$\Gamma(\Phi^j) = \begin{cases} \left(\Phi^j - \underline{\Phi}\right) & \text{if } \underline{\Phi} < \Phi^j < \overline{\Phi} \\ 0 & \text{otherwise} \end{cases} \tag{4}$$

- PRC_2

$$\Gamma(\Phi^j) = \begin{cases} \frac{\Phi^j - \underline{\Phi}}{0.5 - \underline{\Phi}} & \text{if } \underline{\Phi} < \Phi^j < 0.5 \\ 1 - \left(\frac{\Phi^j - 0.5}{\overline{\Phi} - 0.5}\right) & \text{if } 0.5 < \Phi^j < \overline{\Phi} \\ 0 & \text{otherwise} \end{cases} \tag{5}$$

- PRC_3

$$\Gamma(\Phi^j) = \sin^2\left(\pi \Phi^j\right) \tag{6}$$

The various curves are plotted in Fig. 1. PRC_1 (see the black curve, which corresponds to $\underline{\Phi} = -0.1$ and $\overline{\Phi} = 0.9$) has been introduced in Ref. [22] to study the stability of the synchronous regime; its shape has been proposed to mimic a network of leaky integrate-and-fire neurons in the presence of delay (see also Ref. [12]).

The two other PRCs have been selected so as to explore the effect of a progressive regularization of the neuronal response. In particular, we consider the smooth PRC_3 (see Eq. (6)), as a prototype of type I PRC[25,26].

The network dynamics is simulated by implementing the Euler algorithm with a time step $\delta_t = 10^{-3}$. However, in some cases, smaller steps have been considered to avoid problems of spurious synchronization. We typically initialize the phases uniformly in the unit interval, while the fields are initially set equal to zero.

In all cases, we have set $b = 0.8$, $c = 0.1$ and $g = 4 + \sqrt{1000/K}$ (following the existing literature). The last option is justified by the motivation to maintain a balanced regime for $K, N \to \infty$. We have, instead, systematically explored the role of α and β, as the pulse-width is the focal point of this paper. Additionally, the coupling strength μ has been varied, as well as the network-size N, to test for the amplitude of finite-size effects.

The following statistical quantities are used to characterize the emerging dynamical states.

1. *The mean firing rate* is a widely used indicator to quantify the neural activity. It is defined as

$$\nu = \lim_{t \to \infty} \frac{1}{tN} \sum_{j=1}^{N} \mathcal{N}_j(t) \tag{7}$$

where $\mathcal{N}_j(t)$ denotes the number of spikes emitted by the neuron j over a time t.

2. *The coefficient of variations* C_v is a microscopic measure of irregularity of the dynamics based on the fluctuations of the interspike intervals (ISIs). The average C_v is defined as

$$\overline{C}_v = \frac{1}{N} \sum_{j=1}^{N} \frac{\sigma_j}{\tau_j}, \tag{8}$$

where σ_j is the standard deviation of the single-oscillator's ISI, and τ_j is the corresponding mean ISI. If $\overline{C}_v > 1$, then the neurons show a bursting activity, while $\overline{C}_v < 1$ implies that the spike trains is relatively regular.

3. *The order parameter*, χ, is typically used to quantify the degree of synchronisation of a population of neurons[27]. It is defined as

$$\chi^2 \equiv \frac{\overline{\langle \Phi \rangle^2} - \overline{\langle \Phi \rangle}^2}{\langle \overline{\Phi^2} - \overline{\Phi}^2 \rangle}, \tag{9}$$

where $\langle \cdot \rangle$ represents an ensemble average, while overbar is a time average. The numerator is the variance of the ensemble average $\langle \Phi \rangle$, while the denominator is the ensemble mean of the single-neuron's variances. When all neurons behave in exactly the same way (perfect synchronization), then $\chi = 1$. If instead, they are independent, then $\chi \approx 1/\sqrt{N}$. Regimes characterized by intermediate finite values $0 < \chi < 1$ are referred to as instances of partial synchronization. Different regimes are characterized by a χ-value strictly larger than zero; here we are interested in the so-called collective irregular dynamics (CID), characterized by stochastic-like fluctuations of the average $\langle \Phi \rangle$.

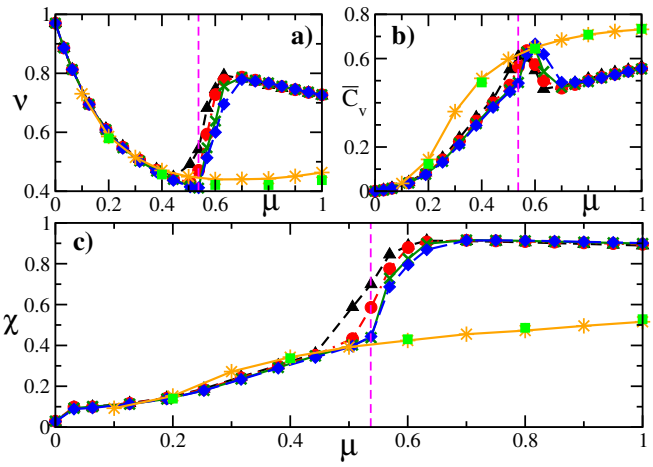

FIG. 2. Characterization of the global network dynamics with interactions through δ pulse, PRC_1 and respectively PRC_3. The mean firing rate ν, mean coefficient of variations $\overline{C}_v$, and order parameter χ vs. coupling strength μ are shown in the panels (a), (b) and (c), respectively. The network size N is encoded in the symbols and color for PRC_1: 10000 (black triangles), 20000 (red circles), 40000 (green crosses), and 80000 (blue diamonds). Similarly for PRC_3: 10000 (orange stars) and 40000 (green squares). The vertical dashed line represents a critical coupling $\mu_c = 0.537$.

III. DELTA PULSE

Most spiking network models deal with δ-spikes, including those giving rise to CID[9,10]. This paper is mostly focused on the more realistic exponential spikes, but before proceeding in that direction we wish to briefly discuss the case of zero pulse-width. This is useful to confirm the ubiquity of CID within the class of pulse-coupled oscillators and as reference to identify possibly new phenomena induced by the presence of finite widths.

δ pulses correspond to the limiting case $\alpha, \beta \to \infty$; they can be treated by invoking Eq. (3). Figure 2 shows the various indicators introduced in Section II, to characterize the collective dynamics. As in previous papers,[9,10] we explore the parameter space, by varying the coupling strength μ and the system size N.

In panel (c) we can appreciate that CID emerges already for very small coupling strength; it is accompanied by an increasing coefficient of variations $\overline{C}_v$, due to the coupling which induces increasing deviations from purely periodic behavior. In parallel, the mean firing rate ν decreases as a result of the prevalent inhibitory character of the network. This weak-coupling emergence of CID is comparable to what observed in balanced LIF models with δ spikes[9].

Above $\mu \approx 0.537 = \mu_c$ (see the vertical dashed lines), a transition occurs towards a highly synchronous regime (χ is slightly smaller than 1), accompanied by a larger firing rate. The corresponding firing activity is mildly irregular: $\overline{C}_v$ is smaller than in Poisson processes (when $\overline{C}_v = 1$). A quick analysis suggests that this self-sustained regime emerges from the vanishing width of the pulses combined with the PRC shape, which is strictly equal to zero in a finite phase range below the threshold $\Phi_{th} = 1$. In fact, similar studies performed with PRC_3 do not reveal any evidence of a phase transition (see orange stars and green squares in Fig. 2) indicating that such behavior is nothing else but a peculiarity of PRC_1 with δ-pulses. We have not further explored this regime. It is nevertheless worth noting that the sudden increase of the firing rate observed when passing to the strong coupling regime is reminiscent of the growth observed in LIF neurons[24], although in such a case, the increase is accompanied by a significantly bursty behavior[28].

More important is the outcome of the finite-size scaling analysis, performed to investigate the robustness of the observed scenario. In Fig. 2 one can see that the various indicators under stimulation of PRC_1 are size-independent deeply within the two dynamical phases, while appreciable deviations are observed in the transition region. This is customary when dealing with phase-transitions. It is not easy to conclude whether the transition is either first or second order: the $\overline{C}_v$ is reminiscent of the divergence of susceptibility seen in continuous transitions, but this is an issue that would require additional work to be assessed.

IV. IDENTICAL FINITE-WIDTH PULSES

In this section, we start our analysis of finite pulses, by assuming the same width for inhibitory and excitatory neurons, i.e. $\alpha^{-1} = \beta^{-1}$. The asymmetric case is discussed in the next section. All other system parameters are kept the same as in the previous section (including the PRC shape).

The resulting phase diagram is reported in Fig. 3. In panel (a) we plot the order parameter χ as a function of μ for different widths: from broad pulses (red stars correspond to $\alpha = 1$, a width comparable to the ISI), down to very short ones (green triangles correspond to $\alpha = 1000$). The general message is that partial synchrony is preserved. Nevertheless, it is also evident that increasing the width progressively decreases the amplitude of the order parameter. The main qualitative difference is the smoothening of the transition observed for δ-pulses (in correspondence of the vertical dashed line at $\mu_c = 0.537$). The singular behavior of δ-spikes is confirmed by the relatively large deviations appearing already for $\alpha = 1000$.

A more direct illustration of the role of α is presented in Fig. 3(b), where we plot χ versus α for different coupling strengths: $\mu = 0.2$ (black triangles), 0.47 (red crosses), and 0.95 (blue diamonds). An overall increasing trend upon shortening the pulse-width is visible for all coupling strengths, although the rate is relatively modest for weak coupling, becoming more substantial in the strong-coupling limit.

Finally, we have briefly investigated the presence of finite-size effects, by performing some simulations for $N = 40000$ (to be compared with $N = 10000$ used in all other simulations): see magenta circles in both panels. We can safely conclude that the overall scenario is insensitive to the network size.

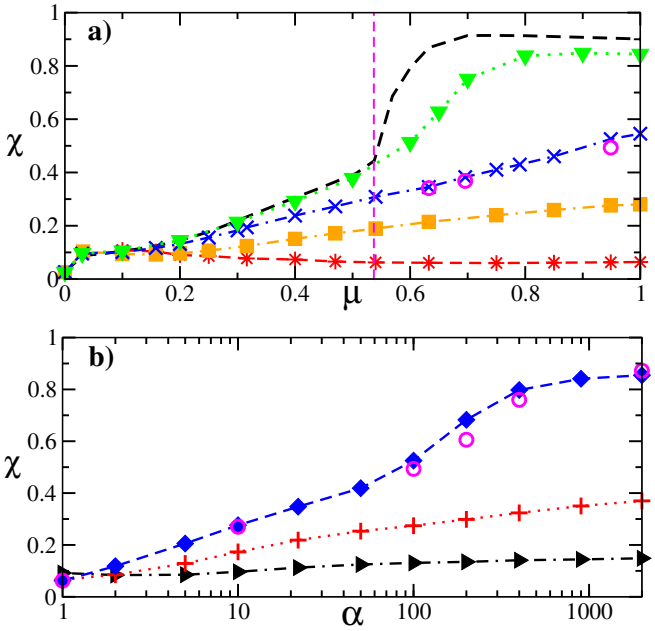

FIG. 3. Characterization of the global network dynamics in the presence of identical pulse-width and PRC_1. Panel a): order parameter χ vs. μ for $N = 10000$ and $\alpha = 1000$ (green triangles), $\alpha = 100$ (blue crosses), $\alpha = 10$ (orange squares), and $\alpha = 1$ (red stars). The black dashed curve corresponds to the asymptotic results obtained for δ pulses (see Fig. 2 (c), $N = 80000$) with the critical value μ_c derived therein. Panel b): order parameter χ vs. α for $N = 10000$ and $\mu = 0.2$ (black triangles), $\mu = 0.47$ (red pluses), and $\mu = 0.95$ (blue diamonds). The horizontal α-axis is in logarithmic scale. In both panels the magenta circles show the results for $N = 40000$ to compare with the blue curves, respectively.

V. FULL SETUP

In the previous section we have seen that the finite width of the spikes does not kill the spontaneous emergence of CID. Here, we analyse the role of an additional element: the asymmetry between inhibitory and excitatory pulses. We proceed by exploring the two-dimensional parameter space spanned by the coupling strength μ and the asymmetry between pulse widths. The latter parameter dependence is explored by setting $\alpha = 100$ and letting β (the inverse width of inhibitory pulses) vary. All other network parameters, including the PRC shape, are assumed to be the same as in the previous section. We start by illustrating the collective dynamics in a system of $N = 40000$ neurons with strong coupling $\mu = 0.95$. Fig. 4 refers to a weakly asymmetric case, $\beta = 95$.

The average phase (see Fig. 4(a)) exhibits stochastic-like oscillations, which represent a first evidence of a non-trivial collective dynamics. The raster plot presented in panel Fig. 4(b) contains the firing times t_n of a subset of 100 neurons: there, one can easily spot the time intervals characterized by a more coordinated action (see, for instance, around time $80 \sim 90$ in Fig. 4(a)). A more quantitative representation is presented in Fig. 4(c), where the instantaneous phase distribution $P(\Phi)$ is plotted at three different times in correspondence of three qualitatively different regimes of the phase dynamics (see the vertical lines in panel (a)). The peak at $\Phi = 0$ is due to the finite fraction of neurons standing still in the refractory period. A small amount of negative phases are also seen: they are due to prevalence of inhibition over excitation at the end of refractoriness. Moreover, the snapshots of the probability density $P(\Phi)$ presented in Fig. 4(c), show that, at variance with the classical asynchronous regime, the shape of the probability density changes with time. The narrowest distribution (blue curve) corresponds to the region where strong regular oscillations of $\langle\Phi\rangle$ are visible in panel (a): within this time interval a "cloud" of neurons homogeneously oscillates from reset to threshold and back.

The results of a systematic numerical analysis are plotted in Fig. 5, where we report three indicators: the firing rate ν, the mean coefficient of variation $\overline{C}_v$, and the order parameter χ, versus β for three different coupling strengths (see the different columns), and four network sizes.

All indicators reveal the existence of two distinct phases: a synchronous regime arising for small β values, and CID observed beyond a critical point which depends on the network size: the transition is discontinuous. All panels reveal a substantial independence of the network size, with the exception of the transition between them (we further comment on this issue later in this section).

The first regime is synchronous and periodic, as signalled by $\chi = 1$, and $\overline{C}_v = 0$. The corresponding firing rate ν is a bit smaller than 0.97, the value expected in the limit of uncoupled neurons (taking into account refractoriness). This is consistent with the expected predominance of inhibition over excitation in this type of setup. A closer look shows that in the synchronous regime ν increases with β. This makes sense since the smaller β, the longer the time when inhibition prevails thereby decreasing the network spiking activity. The weak dependence of ν on the coupling strength μ is a consequence of small effective fields felt by neurons when the PRC is small. Finally, for intermediate β values (around 80) and large coupling strengths, χ is large but clearly smaller than 1. This third type of regime will be discussed in the next section.

CID is characterized by a significantly smaller order parameter which, generally tends to increase with the coupling strength. CID is also characterized by a significantly smaller firing rate. This is due the prevalence of inhibition which is not diminished by the refractoriness as in the synchronous regime. Finally, the coefficient of variation is strictly larger than 0, but significantly smaller than 1 (the value of Poisson processes) revealing a limited irregularity of the microscopic dynamics. In agreement with our previous observations for δ-spikes, $\overline{C}_v$ increases with the coupling strength.

Our observation of an irregular regime for $\beta < \alpha$ are in line with the numerical observations discussed in Ref. [20], with reference to LIF neurons and with the hypothesis that a slower inhibitory activity might lead to rhythmic oscillations[29]. On the other hand, our finite-size scaling analysis also shows that the degree of asymmetry (between pulse widths) compatible with CID progressively reduces upon increasing the number of neurons. Although the N-dependence varies significantly with the coupling strength, it is natural to conjecture that,

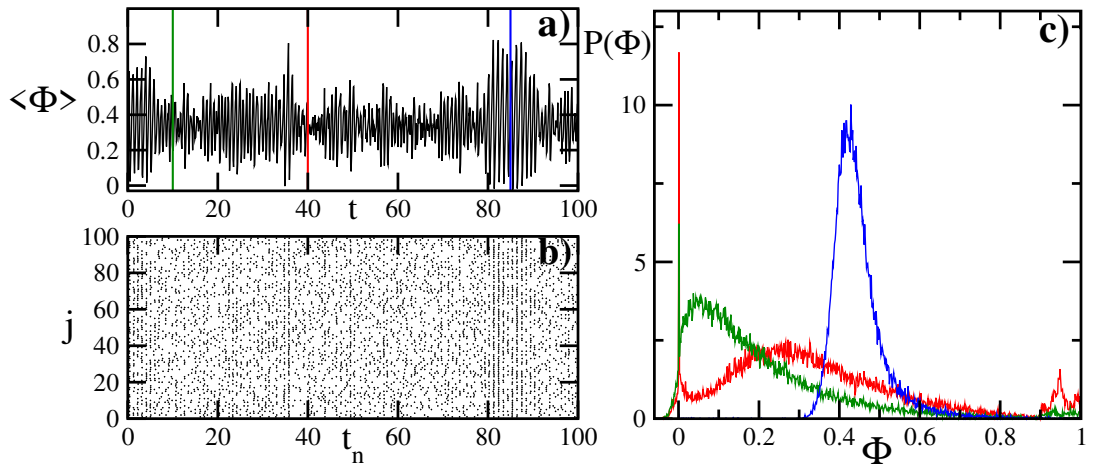

FIG. 4. Microscopic phase dynamics for nonidentical pulse-width. All presented data refers to PRC_1, $\mu = 0.95$, $\alpha/\beta = 100/95$ and $N = 40000$. Panel a): the time series for average membrane potential (phase) after the transient has sorted out. Panel b): the rastergram of spiking times t_n for 100 oscillators out of $N = 40000$. Panel c): the instantaneous probability distribution of the phases $P(\Phi)$ at three different time points $t = 10$ (green), $t = 40$ (red), and $t = 85$ (blue) time units. The curves are normalized such that the area underneath is 1.

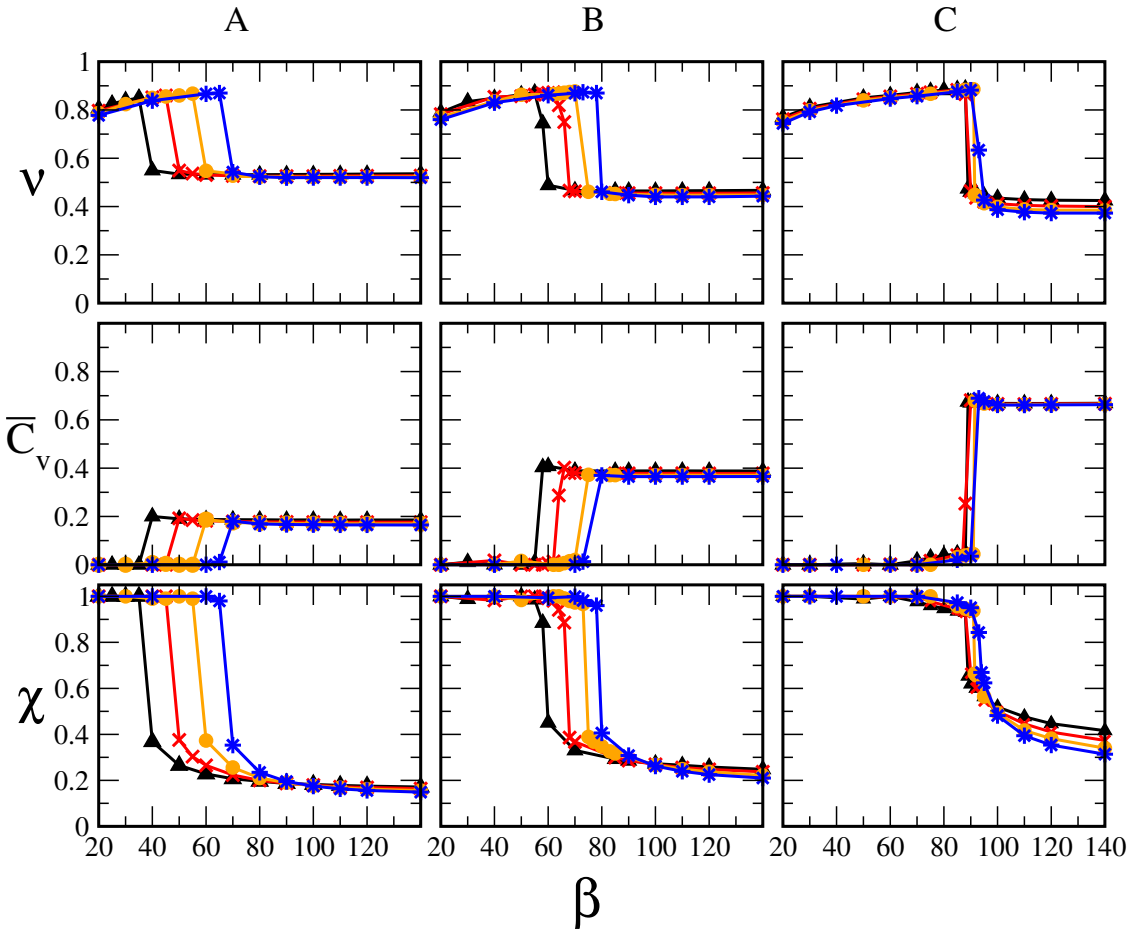

FIG. 5. Characterization of the global network dynamics for nonidentical pulse-width and PRC_1. Each column refers to different coupling strengths: $\mu = 0.3$ (A), $\mu = 0.47$ (B), and $\mu = 0.95$ (C). Rows: mean firing rate ν, mean coefficient of variations $\overline{C}_v$, and order parameter χ versus β. Colours and symbols in all panels define various network sizes N: 10000 (black triangles), 20000 (red crosses), 40000 (orange circles), and 80000 (blue stars). Each data point is based on a time series generated over 10000 time units and sampled every 1000 steps after the transient has sorted out.

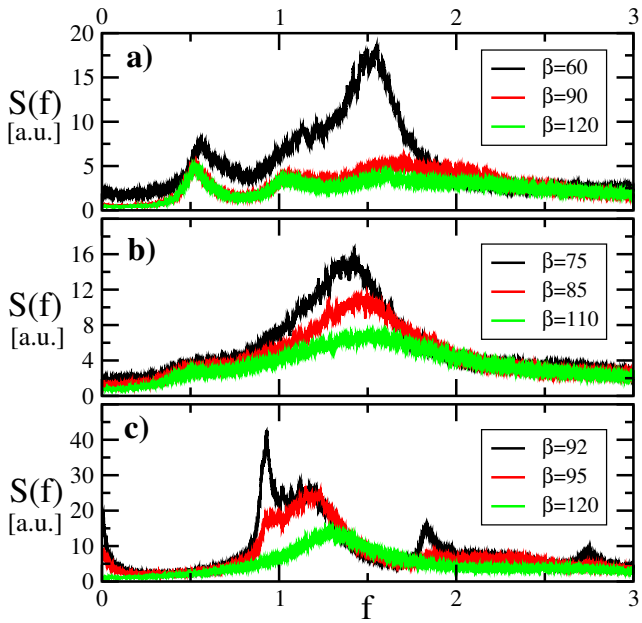

FIG. 6. Power spectra of average membrane potential as function of frequency. All presented data refers to PRC_1, $\alpha = 100$ and $N = 40000$. Each panel corresponds to different μ: 0.3 (a), 0.47 (b), and 0.95 (c).

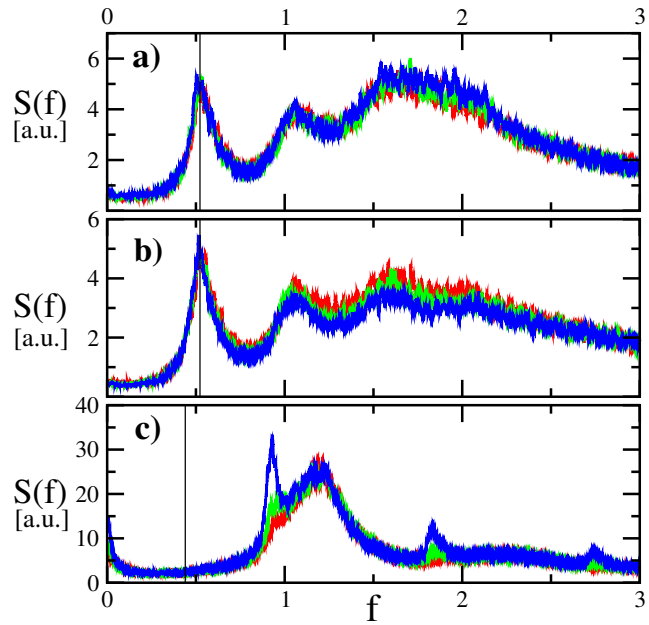

FIG. 7. Power spectra of average membrane potential as function of frequency. Panel: a) $\beta = 90$, $\mu = 0.3$, b) $\beta = 120$, $\mu = 0.3$ and c) $\beta = 95$, $\mu = 0.95$. Each colour in all panels refers to different network size N: 20000 (red), 40000 (green), and 80000 (blue). All presented data refers to PRC_1 and $\alpha = 100$. The vertical line is pointing out the mean firing rate $\nu \approx 0.523$ for $\mu = 0.3$ and $\nu \approx 0.44$ for $\mu = 0.95$ (see Fig.5).

asymptotically, CID survives only for $\beta \geq \alpha$. This is not too surprising from the point of view of self-sustained balanced states. They are expected to survive only when inhibition and excitation compensate each other: the presence of different time scales makes it difficult, if not impossible to ensure a steady balance.

We conclude this section with a more quantitative characterization of the irregularity of the collective dynamics. In Fig. 6, we plot the Fourier power spectrum $S(f)$ obtained from $\langle\Phi\rangle(t)$. The panels correspond to three different coupling strengths ($\mu = 0.3$, 0.47 and 0.95, from top to bottom). For each value of μ, we have sampled three different pulse-widths.

Altogether, one can notice a general increase of the power with μ. This is quite intuitive, as CID is the result of mutual interactions. A less obvious phenomenon is the increase of the power observed when the inhibitory pulse-width β^{-1} is increased. This is an early signature of a transition towards full synchronization, observed when β is decreased below a critical value. Anyway, the most important message conveyed by Fig. 6 is that all spectra exhibit a broadband structure, although most of the power is concentrated around a specific frequency: $f \approx 1.5$ (panel a), $f \approx 1.4$ (panel b), and $f \approx 0.93$ (panel c). As a result, one can preliminarily conclude that the underlying macroscopic evolution is stochastic-like. A more detailed analysis could be performed by computing macroscopic Lyapunov exponents, but this is an utterly difficult task, as it is not even clear what a kind of equation one should refer to.

Additional evidence of the robustness of CID is given in Fig. 7, where we investigate the amplitude of finite-size corrections, by computing the power spectrum $S(f)$ for different network sizes for three different parameter sets: $\mu = 0.3$, $\beta = 90$ (panel a), $\mu = 0.3$, $\beta = 120$ (panel b), and $\mu = 0.95$, $\beta = 95$ (panel c). In all cases, the spectra are substantially independent of the number of neurons, although in panel (b) we observe a weak decrease in the band $f \in [1, 2.5]$, while a new set of peaks is born in panel (c). Since the connectivity K of the largest networks herein considered ($N = 80,000$) is comparable to that of the mammalian brain (K =8000 vs 10000[4]), we can at least conjecture that this phenomenon may have some relevance in realistic conditions.

Finally, the low frequency peak clearly visible for small μ coincides with the mean firing rate (see Fig. 5(a)), while the connection with the microscopic firing rate is lost in panel (c).

VI. TRANSITION REGION

In the previous section we have seen a clear evidence of a first-order phase transition, when either the pulse-width or the coupling strength is varied. So far, each simulation has been performed by selecting afresh a network structure. The stability of our results indicates that the transition does not suffer appreciable sample-to-sample fluctuations.

The main outcome of our numerical simulations is summarized in Fig. 8; the various lines identify the transition between the two regimes, for different network sizes. The critical points have been determined by progressively decreasing

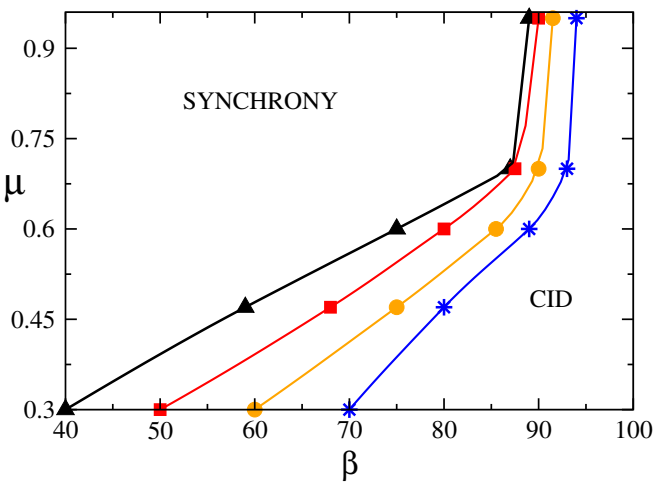

FIG. 8. Phase diagram for different network sizes N: 10000 (black triangles), 20000 (red squares), 40000 (orange circles), and 80000 (blue stars).

β (see Fig. 5) and thereby determining the minimum β-value where CID is stable. Upon increasing N, the synchronization region grows and the transition moves towards $\beta = \alpha$.

So far, the initial condition has been fixed by selecting independent, identically uniformly distributed random phases and zero fields. Since it is known that discontinuous transitions are often accompanied by hysteretic phenomena, we now explore this question. Fig. 9 combines results presented in the previous section for a network with $N = 10000$ neurons and $\mu = 0.3$ (the blue dots reproduce the content of Fig. 5A), with new indicators introduced here below.

The first insight comes from the evolution of nearly synchronous states. In this case, the initial phases are selected within a small interval of width δ_p (while the fields are set equal to zero and $\delta_t = 10^{-4}$).[30] The resulting values of the various observables for $\delta_p = 10^{-3}$ are reported in Fig. 9: see the black curves and triangles. The most relevant result is the discovery of a wide range of β-values, where the order parameter is either exactly equal to 1 or close to it. This implies the presence of a bistability between CID and a stable quasi-synchronous solution with a small basin of attraction.

Linear-stability analysis of the periodic synchronous state provides some relevant informations. The conditional Lyapunov exponent λ_c can be determined in a semi-analytic form: its expression for PRC_1 is derived in Appendix (A): see Eq. (A8). The results are presented in Fig. 9(c) (see the red curve): there we see that when the synchronous solution is transversally unstable, the quasi-synchronous regime systematically arises. However, the reverse is not true: there are β values where the synchronous state is stable and yet CID is observed. The inconsistency is partially solved by looking at a more accurate quantifier of the stability of the periodic solution: the exact maximal Lyapunov exponent λ. By following the approach developed in Ref. [22], λ can be determined by computing the eigenvalues of a suitable random matrix. The implementation of this method leads to the green curve, slightly above the conditional Lyapunov exponent. The new curve partially closes the gap between the stability limit of the periodic state and the onset of CID, but the general scenario is still unclear.

A careful look allows identifying the dynamical regimes according to different β intervals. The first one comes from the observation of random ICs: $[42, 120]$ is characterized by stable CID (see blue circles in Fig. 9(c)). Below $\beta \approx 42$ the irregular dynamics collapses into periodic states. As confirmed by the finite-width perturbation analysis (black triangles in Fig. 9(c)), the periodic dynamics is stable over a range $[20, 40]$ followed by a hysteretic behaviour in $[41, 106]$. In the latter interval, depending on the initial condition, one can either observe CID or periodic states. Understanding the nature of the transition from CID to synchrony would require additional work.

More specifically, $[20, 46)$ is characterized by the fully synchronous dynamics. This is consistent with the linear stability analysis, which also shows that $\beta \approx 46$ is the value beyond which the synchronous state becomes unstable (see the λ curve).

Symmetrically, for $\beta \in [90, 106]$, we observe the simultaneous presence of CID and full synchrony in a region where the synchronous-state stability is restored (see again λ). The basin of attraction for the fully and quasi-synchronous solution is quite small in the range $\beta \in [41, 106]$ and relies on a sufficient small spread in the initial conditions δ_p. For $\delta_p \geq 0.2$ the system converges to CID.

Much less intuitive is the regime observed for $\beta \in [46, 90]$. In that range, the fully synchronous solution is linearly unstable, but yet the phases remain confined to a small region and quasi-synchrony is stable. The phenomenon is a combined effect of refractoriness and the shape of the PRC. As we suspect it to be rather peculiar, we do not investigate in detail but limit ourselves to illustrate it in Fig. 10, where we report four snapshots of the phase distributions close to the β value, where this regime ceases to exist. The width of the various distributions progressively shrinks while approaching the critical point, where the synchronous state becomes stable: the green curve, which corresponds to $\beta = 46.3$, is almost δ-like. The mechanism responsible for the loss of stability of this quasi-synchronous regime at the other edge of the interval $[46, 90]$ appears to be different and further studies would be required.

Finally, we have performed numerical studies with broader pulses, to test the robustness of our findings. More precisely, now we assume the pulse-widths α^{-1}, β^{-1} to be longer than the refractory time t_r as observed in real neurons[4,24]. The results are displayed in Fig. 11 for $\alpha = 12$ and $\mu = 0.3$. Once again, we see that CID extends to the region where $\beta < \alpha$ and that the transition point moves progressively towards $\beta = \alpha$ upon increasing the network size (see the different curves). On the other hand the strength of CID is significantly low ($\chi = 0.11$), possibly due to the relative smallness of the coupling strength. Furthermore, the evolution of quasi-synchronous solutions ($\delta_p = 10^{-3}$), reveals again bistability in a relatively wide interval of β-values, $\beta \simeq 8.5 - 14.3$, which now extends beyond $\beta = \alpha$: a result, compatible with the transversal stability (see the red curve for λ_c in Fig. 11).

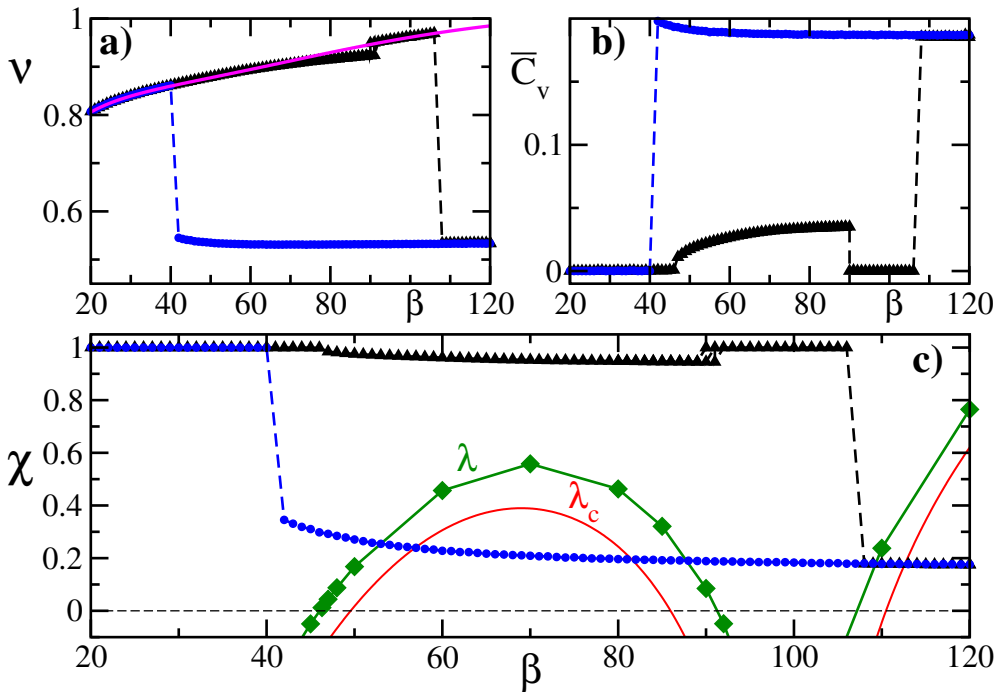

FIG. 9. The emergence of a bistable regime for nonidentical pulse widths and PRC$_1$. The parameter set is the same as in Fig. 5A with $N = 10000$. Panels: a) mean firing rate ν, b) mean coefficient of variations $\overline{C}_v$, and c) order parameter χ versus β. The blue circles and black triangles in all panels correspond to the full network with a full range (uniform) and narrow ICs, respectively. The narrow ICs are chosen to be in the order of $\delta_p = 10^{-3}$. The green diamonds corresponds to the maximal Lyapunov exponent, and the red one is the conditional Lyapunov exponent as function of β. The magenta line (a) represents the semi analytic firing rate given in Eq.A2. The horizontal dashed line (c) is a reference point ($\lambda = 0$) in which the synchronous state changes its stability.

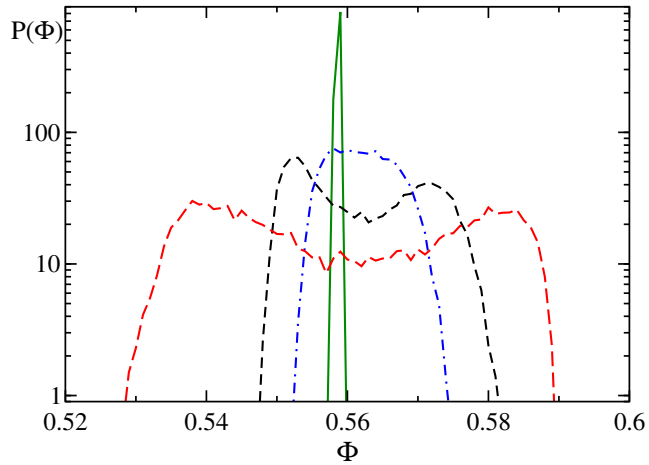

FIG. 10. The instantaneous probability distribution P(Φ) at particular time point. Colour and shape define different β values ordered from the widest to the narrowest distribution: 70 (red), 50 (black), 48 (blue), and 46.3 (green). All snapshots are corresponding to the black triangles in Fig. 9. The vertical axis is in the logarithmic scale. The curves are normalized such that the area underneath is 1.

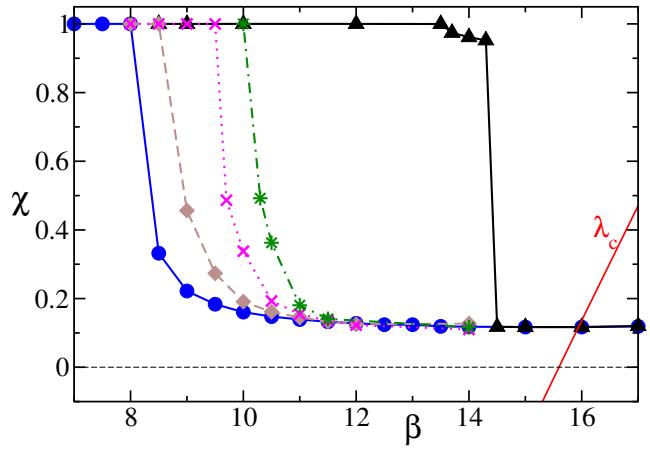

FIG. 11. Characterization of the global network dynamics for long pulse width and PRC$_1$. The parameters $\mu = 0.3$ and $\alpha = 12$ are fixed. The blue circles ($N = 10000$), brown diamonds ($N = 20000$), magenta cross ($N = 40000$), and green stars ($N = 80000$) correspond to the full range and random ICs. The black triangles ($N = 10000$) correspond to narrow ICs with $\delta_p = 10^{-3}$. The red curve is the conditional Lyapunov exponent.

A. Robustness

In the previous sections we have investigated the dependence of CID on the spike-width as well as on the coupling strength. Now, we examine the role of the PRC shape. Following Fig. 1, we consider a couple of smoothened versions of PRC$_1$, defined in section II. The results obtained for a net-

work of $N = 10000$ neurons are reported in Fig. 12.

All simulations have been performed for $\alpha = 100$, while β has been again varied in the range $[40, 120]$. In each panel, blue circles, orange stars and green diamonds have been obtained by setting $\mu = 0.3$; they correspond to $PRC_{1,2,3}$ respectively. As a first general remark, the overall scenario is not strongly affected by the specific shape of the PRC. The mean firing rate is approximately the same in all cases, while the coefficient of variation is substantially higher for the sinusoidal (and more realistic) PRC_3. Moreover, the order parameter for PRC_3 is remarkably close to that for PRC_1 (see panel c).

The most substantial difference concerns the transition from synchrony to CID, which occurs much earlier in PRC_2. On the other hand, the χ-behavior of PRC_2 can be brought to a much closer agreement by increasing the coupling strength (the green asterisks in Fig. 12 refer to $\mu = 0.7$). This observation raises the issue of quantifying the effective amplitude of the coupling: PRCs are introduced in Sec. II are all functions whose maximum value is equal to 1. This does not exclude that the effective amplitude may be significantly different, deviation that can be partially removed by adjusting the value of the coupling constant μ as shown in Fig. 12.

Anyhow, these qualitative arguments need a more solid justification. In fact, one can also notice that in this last case (PRC_2 and $\mu = 0.7$) $\overline{C}_v$ is significantly larger (above 0.6 instead of below 0.2), consistently with the analysis carried out in Ref. [28], where it is shown that a large coupling strentgh induces a bursting phenomena in LIF neurons.

Finally, we investigate the presence of hysteresis in the case of PRC_3. The results, obtained by setting all parameters as in the previous cases, are reported in Fig. 12 (see black triangles): they have been obtained by setting the initial spread of phases $\delta_p = 10^{-3}$. Once again, there exists a wide parameter range where CID coexists with a stable synchronous regime. At variance with the previous case (see Fig. 9), the synchronous state is always stable over the range $\beta \leq 110$. This is consistent with the behavior of the conditional Lyapunov exponent, which, at variance with PRC_1, does not exhibit an “instability island". As from Eq. (A8), λ_c is the sum of two terms. In the case of PRC_3, the second one is absent because the PRC amplitude is zero at the reset value $\Phi_r = 0$.

VII. CONCLUSION AND OPEN PROBLEMS

In this paper we have discussed the impact of finite pulse-widths on the dynamics of a weakly inhibitory neuronal network, especially with reference to the sustainment and stability of the balanced regime. We have considered the simplest case, namely exponential pulses, whose simulation requires just one variable per field (excitatory/inhibitory) per neuron. We have found that the collective irregular dynamics persists, at least in so far as the width of the spikes is small compared to the average interspike intervals (as it happens in reality).

The stability analysis of the synchronous regime, together with direct numerical simulations, reveals a crucial role played by the asymmetry between excitatory and inhibitory spikes. Indeed, the case of identical pulse-widths is very peculiar (degenerate), as the balance between inhibition and excitation is automatically maintained over different time scales. On the other hand, different pulse-widths imply that either excitation or inhibition may prevail over different time ranges, potentially breaking the balance. This is particularly evident in the synchronous regime where the overall field is the superposition of two suitably weighted exponential shapes with opposite sign: depending on the time, the effective field may change sign signalling a prevalence of either inhibition or excitation.

Altogether CID is robust when inhibitory pulses are shorter than excitatory ones (this is confirmed by the corresponding instability of the synchronous regime). More intriguing is the scenario observed in the opposite case, when CID and synchrony maybe simultaneously stable. A finite-size analysis performed by simulating increasingly large networks shows that the hysteretic region progressively shrinks, although it is still prominent - especially for weak coupling - for $N = 80,000$, when the connectivity of our networks ($K = 8,000$) is comparable to that of the mammalian brain. Anyhow, on a purely mathematical level, one can argue that the transition from CID to synchrony eventually occurs for identical widths.

Further studies are definitely required to build a general scenario, since the dynamics depends on several parameters. Here, we have explored in a preliminary way the role of the PRC shape: so long as it is almost of Type I, the overall scenario is robust.

Finally, the transition from CID to synchrony still requires more indepth studies. A possible strategy consists in mimicking the background activity as a pseudo-stochastic process, thereby writing a suitable Fokker-Planck equation. However, at variance with the δ-spike case, here additional variables would be required to account for the inhibitory/excitatory fields.

ACKNOWLEDGMENTS

Afifurrahman was supported by the Ministry of Finance of the Republic of Indonesia through the Indonesia Endowment Fund for Education (LPDP) (grant number: PRJ-2823/LPDP/2015).

DATA AVAILABILITY

The data that support the findings of this study are available from the corresponding author upon reasonable request.

Appendix A: Mean field model for finite-width pulse

We investigate the stability of the period-1 synchronous state through the conditional Lyapunov exponent. This regime is characterised by a synchronous threshold-passing of all oscillators leading to exactly the same exponentially decaying excitatory and inhibitory field for all oscillators. The synchronous solution $\Phi(t)$ with a period T of Eqs. (1,2) is ob-

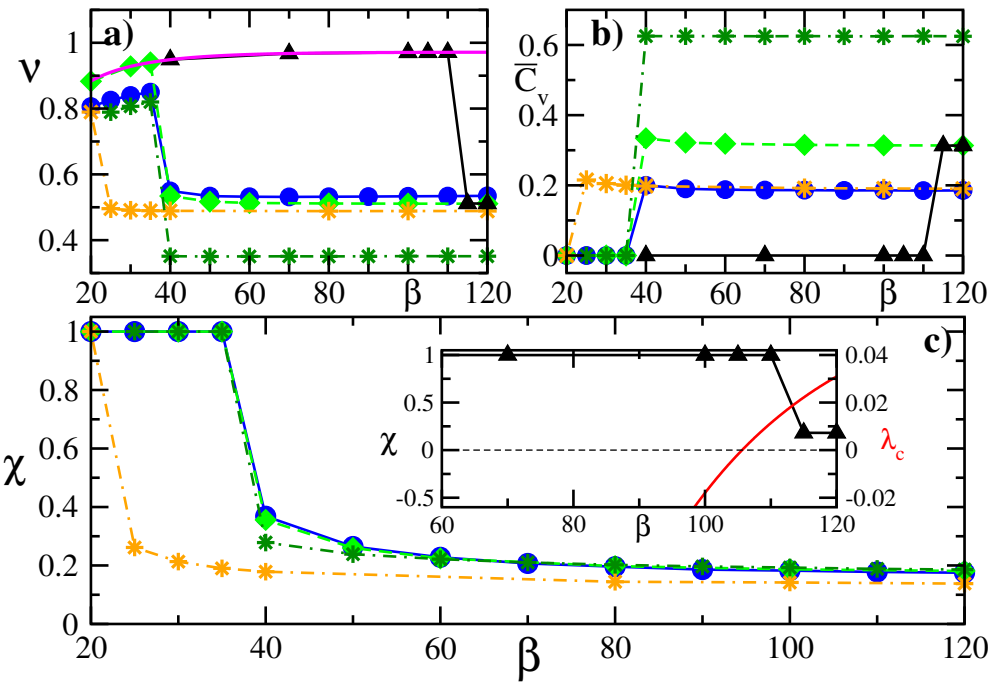

FIG. 12. The emerging scenario for different PRCs with $\mu = 0.3$ (in addition $\mu = 0.7$ is the exemption for PRC_2), $\alpha = 100, N = 10000$. Panels: a) mean firing rate ν, b) mean coefficient of variations $\overline{C}_v$, and c) order parameter χ vs. β. Blue circles correspond to PRC_1, orange stars PRC_2, green stars PRC_2 with $\mu = 0.7$, green diamond PRC_3. Inset: a bistable regime emerges for PRC_3 in a network of $N = 10000$ neurons with $\delta_p = 10^{-3}$ (black triangels) accompanied by the conditional Lyapunov exponent (red curve). The magenta curve (panel a) represents the semi-analytic firing rate for PRC_3 according to Eq.A2.

tained by integrating the equation

$$\begin{cases} \dot{\Phi} & = 1 + \frac{\mu}{\sqrt{K}}\Gamma(\Phi)(E(t) - I(t)) \\ E(t) & = E_\circ e^{-\alpha t} \\ I(t) & = I_\circ e^{-\beta t} \end{cases} \tag{A1}$$

where

$$E_\circ = \frac{K_e \alpha}{1 - e^{-\alpha T}}, \qquad I_\circ = \frac{g K_i \beta}{1 - e^{-\beta T}}.$$

The fields follow an exponential decay with the initial amplitudes $E_\circ, I_\circ$ for the excitatory and inhibitory field, respectively. In order to determine the stability of the synchronous state, we first need to find the period T via a self-consistent iterative approach. Setting the origin $t = 0$ to the time point when the phase has been reset to zero, we define T as a time point in which the phase variable reaches its maximal value i.e. $\Phi(T) = 1$. We integrate the phase starting from $\Phi = 0$ up to $\Phi(T)$ by initially imposing arbitrary non-zero values for $E_\circ$ and $I_\circ$. The period T is used to restart the procedure with refined estimate of the initial field amplitudes $E_\circ, I_\circ$, until convergence to a fixed point is ensured. The firing rate is given by,

$$\tilde{\nu} \equiv \frac{1}{T} \tag{A2}$$

The conditional (also known as transversal) Lyapunov exponent is a simple tool to assess the stability of the synchronous regime. It quantifies the stability of a single neuron subject to the external periodic modulation resulting from the network activity. The transversal, or conditional Lyapunov exponent is the growth rate λ_c of an infinitesimal perturbation. Let us now denote with δt_r the time shift at the end of a refractory period. The corresponding phase shift is[22]

$$\delta\phi_r = \dot{\Phi}(t_r)\delta t_r = \left\{1 + \frac{\mu}{\sqrt{K}}\Gamma(0)[E(t_r) - I(t_r)]\right\}\delta t_r\,. \tag{A3}$$

From time t_r up to $\bar{t}$ the phase shift evolves according to,

$$\dot{\delta\phi} = \frac{\mu}{\sqrt{K}}\Gamma'(\Phi)(E(t) - I(t))\delta\phi\,, \tag{A4}$$

where $\bar{t}$ is the minimum between the time when PRC_1 drops to zero and the time when the threshold is reached (in either case, we neglect the variation of field dynamics, since the field is treated as an external forcing). As a result,

$$\delta\phi = e^D \delta\phi_r\,, \tag{A5}$$

where,

$$D = \int_{t_r}^{\bar{t}} \frac{\mu}{\sqrt{K}}\Gamma'(\Phi)(E(t) - I(t))dt. \tag{A6}$$

The corresponding time shift is

$$\overline{\delta t} = \frac{\delta\phi}{\dot{\bar{\Phi}}}$$

where $\dot{\bar{\Phi}}$ is the velocity at $\bar{t}$. The shift $\overline{\delta t}$ carries over unchanged until first the threshold $\Phi_{th} = 1$ is crossed and then the new refractory period ends. Accordingly, from Eqs. (A3,A5), the expansion R of the time shift over one period (a sort of Floquet multiplier) can be written as

$$R = \frac{\overline{\delta t}}{\delta t_r} = \frac{1 + \frac{\mu}{\sqrt{K}}\Gamma(0)[E(t_r) - I(t_r)]}{\dot{\bar{\Phi}}} \mathrm{e}^D \qquad \text{(A7)}$$

This formula is substantially equivalent to Eq. (54) of Ref. [31] (Λ_{ii} corresponds to R), obtained while studying a single population under the action of α-pulses. An additional marginal difference is that while in Ref. [31] the single neuron dynamics is described by a non uniform velocity field $F(x)$ and homogeneous coupling strength, here we refer to a constant velocity and a phase-dependent PRC, $\Gamma(\Phi)$.

The corresponding conditional Lyapunov exponent is

$$\lambda_c = \frac{\ln|R|}{T} = \frac{D + \ln\left|[1 + \frac{\mu}{\sqrt{K}}\Gamma(0)(E(t_r) - I(t_r))]/\dot{\bar{\Phi}}\right|}{T}. \qquad \text{(A8)}$$

The formula (A8) is valid for all PRCs as long as $\bar{t}$ is replaced by T. The formula (A8) is the sum of two contributions: the former one accounts for the linear stability of the phase evolution from reset to threshold (D/T); the latter term arises from the different velocity (frequency) exhibited at threshold and at the end of the refractory period. Notice that in the limit of short pulses, the field amplitude at time $\bar{t}$ is effectively negligible, and one can thereby neglect the effect of the fields and assume $\dot{\bar{\Phi}} = 1$.

In mean-field models, the conditional Lyapunov exponent coincides with the exponent obtained by implementing a rigorous theory which takes into account mutual coupling.

[1] B. Jarosiewicz, B. L. McNaughton, and W. E. Skaggs, "Hippocampal population activity during the small-amplitude irregular activity state in the rat," Journal of Neuroscience **22**, 1373–1384 (2002), https://www.jneurosci.org/content/22/4/1373.full.pdf.

[2] S. Shinomoto, H. Kim, T. Shimokawa, N. Matsuno, S. Funahashi, K. Shima, I. Fujita, H. Tamura, T. Doi, K. Kawano, and et al., "Relating neuronal firing patterns to functional differentiation of cerebral cortex," PLoS Computational Biology **5**, e1000433 (2009).

[3] W. Truccolo, L. R. Hochberg, and J. P. Donoghue, "Collective dynamics in human and monkey sensorimotor cortex: predicting single neuron spikes," Nature Neuroscience **13**, 105–111 (2009).

[4] W. Gerstner, W. M. Kistler, R. Naud, and L. Paninski, *Neuronal Dynamics: From Single Neurons to Networks and Models of Cognition* (Cambridge University Press, USA, 2014).

[5] C. van Vreeswijk and H. Sompolinsky, "Chaos in neuronal networks with balanced excitatory and inhibitory activity," Science **274**, 1724–1726 (1996).

[6] C. v. Vreeswijk and H. Sompolinsky, "Chaotic balanced state in a model of cortical circuits," Neural Computation **10**, 1321–1371 (1998), https://doi.org/10.1162/089976698300017214.

[7] N. Brunel, "Dynamics of sparsely connected networks of excitatory and inhibitory spiking neurons," Journal of Computational Neuroscience **8**, 183–208 (2000).

[8] S. Luccioli and A. Politi, "Irregular collective behavior of heterogeneous neural networks," Physical Review Letters **105** (2010), 10.1103/PhysRevLett.105.158104.

[9] E. Ullner, A. Politi, and A. Torcini, "Ubiquity of collective irregular dynamics in balanced networks of spiking neurons," Chaos: An Interdisciplinary Journal of Nonlinear Science **28**, 081106 (2018), https://doi.org/10.1063/1.5049902.

[10] A. Politi, E. Ullner, and A. Torcini, "Collective irregular dynamics in balanced networks of leaky integrate-and-fire neurons," The European Physical Journal Special Topics **227**, 1185–1204 (2018).

[11] A. Pikovsky and M. Rosenblum, "Dynamics of globally coupled oscillators: Progress and perspectives," Chaos: An Interdisciplinary Journal of Nonlinear Science **25**, 097616 (2015), https://doi.org/10.1063/1.4922971.

[12] E. Ullner and A. Politi, "Self-sustained irregular activity in an ensemble of neural oscillators," Phys. Rev. X **6**, 011015 (2016).

[13] E. Montbrió, D. Pazó, and A. Roxin, "Macroscopic description for networks of spiking neurons," Phys. Rev. X **5**, 021028 (2015).

[14] R. Zillmer, R. Livi, A. Politi, and A. Torcini, "Desynchronization in diluted neural networks," Phys. Rev. E **74**, 036203 (2006).

[15] S. Jahnke, R.-M. Memmesheimer, and M. Timme, "Stable irregular dynamics in complex neural networks," Phys. Rev. Lett. **100**, 048102 (2008).

[16] R. Zillmer, N. Brunel, and D. Hansel, "Very long transients, irregular firing, and chaotic dynamics in networks of randomly connected inhibitory integrate-and-fire neurons," Phys. Rev. E **79**, 031909 (2009).

[17] A. Politi and A. Torcini, "Stable chaos," in *Nonlinear dynamics and chaos: advances and perspectives*, Underst. Complex Syst. (Springer, Berlin, 2010) pp. 103–129.

[18] C. C. Canavier, *Encyclopedia of Computational Neuroscience*, edited by D. Jaeger and R. Jung (Springer New York, New York, NY, 2013) pp. 1–11.

[19] R. Zillmer, R. Livi, A. Politi, and A. Torcini, "Stability of the splay state in pulse-coupled networks," Phys. Rev. E **76**, 046102 (2007).

[20] D.-P. Yang, H.-J. Zhou, and C. Zhou, "Co-emergence of multi-scale cortical activities of irregular firing, oscillations and avalanches achieves cost-efficient information capacity," PLOS Computational Biology **13**, 1–28 (2017).

[21] W. Gerstner and W. Kistler, *Spiking Neuron Models: An Introduction* (Cambridge University Press, New York, NY, USA, 2002).

[22] Afifurrahman, E. Ullner, and A. Politi, "Stability of synchronous states in sparse neuronal networks," Nonlinear Dynamics **102**, 733–743 (2020).

[23] D. Golomb, D. Hansel, and G. Mato, "Chapter 21 mechanisms of synchrony of neural activity in large networks," in *Neuro-Informatics and Neural Modelling*, Handbook of Biological Physics, Vol. 4, edited by F. Moss and S. Gielen (North-Holland, 2001) pp. 887 – 968.

[24] S. Ostojic, "Two types of asynchronous activity in networks of excitatory and inhibitory spiking neurons," Nature Neuroscience **17**, 594–600 (2014).

[25] C. C. Canavier, "Phase response curve," Scholarpedia **1**, 1332 (2006).

[26] E. M. Izhikevich and B. Ermentrout, "Phase model," Scholarpedia **3**, 1487 (2008).

[27] D. Golomb, "Neuronal synchrony measures," Scholarpedia **2**, 1347 (2007).

[28] E. Ullner, A. Politi, and A. Torcini, "Quantitative and qualitative analysis of asynchronous neural activity," Phys. Rev. Research **2**, 023103 (2020).

[29] X.-J. Wang, "Neurophysiological and computational principles of cortical rhythms in cognition," Physiological Reviews **90**, 1195–1268 (2010), pMID: 20664082, https://doi.org/10.1152/physrev.00035.2008.

[30] In the simulations, it is crucial to fix the time-step δ_t at least ten times smaller than δ_p, in order to ensure that the spike times are properly handled during the integration process.

[31] S. Olmi, A. Politi, and A. Torcini, "Linear stability in networks of pulse-coupled neurons," Frontiers in Computational Neuroscience **8**, 8 (2014).